crystals

MDPI

Article

Temperature Dependence of the Thermal, Electrical Resistivity, Dielectric and Piezoelectric Properties of $CaYAl_3O_7$ Crystal

Yang Li, Zhitai Jia *, Yanru Yin, Qiangqiang Hu, Wenxiang Mu, Jian Zhang, Xiaoqiang Yu and Xutang Tao *

State Key Laboratory of Crystal Materials & Key Laboratory of Functional Crystal Materials and Device, Shandong University, Jinan 250100, China; yanglisdu@126.com (Y.L.); mythicgirl@163.com (Y.Y.); q.hu@sdu.edu.cn (Q.H.); muwenxiang2013@gmail.com (W.M.); jian.zhang@sdu.edu.cn (J.Z.); yuxq@sdu.edu.cn (X.Y.)

* Correspondence: z.jia@sdu.edu.cn (Z.J.); txt@sdu.edu.cn (X.T.)

Received: 13 December 2017; Accepted: 10 January 2018; Published: 14 January 2018

Abstract: Calcium yttrium aluminate ($CaYAl_3O_7$) crystal was grown and characterized in detail for high temperature piezoelectric sensors for the first time. The thermal properties of the $CaYAl_3O_7$ (CYAM) crystal were investigated systematically. In particular, the CYAM crystal exhibits considerably high resistivity along X- and Z- direction in the order of 6.96×10^7 Ω·cm and 2.86×10^8 Ω·cm at 600 °C, respectively. The temperature dependence of the electromechanical properties of CYAM crystal were investigated over the temperature range of 25–500 °C. The high thermal stability of piezoelectric properties together with its high electrical resistivity, makes $CaYAl_3O_7$ crystal a promising candidate for high temperature piezoelectric applications.

Keywords: piezoelectric materials; melilite crystals; high temperature applications

1. Introduction

Currently, electromechanical devices have been designed and extensively used in various electronic devices such as actuators, sensors, and transducers. Innovations in electromechanical devices continue to be the main driving force for the exploration of novel piezoelectric materials, especially in a high-temperature and harsh environment [1–4]. Nowadays, from the perspective of practical application, developing lead-free piezoelectric materials with the merits of high electrical resistivity, low dielectric loss, large piezoelectric coefficient and high temperature stability are desirable for wide range of high-temperature sensor applications [5–8]

Recently, melilite crystals with formula of ABC_3O_7, which belong to the tetragonal system with space group of $P\bar{4}2_1m$, has attracted much attention in high temperature piezoelectric investigations. Here, A = Ca, Sr, Ba; B = La, Gd; and C = Al, Ga, respectively [9–11]. In general, the ABC_3O_7 family presents no phase transition up to their melting point (1500~1700 °C), exhibiting good piezoelectric properties without pyroelectricity [12]. Furthermore, melilite crystals can be grown from melt by Cz technique. As reported, $SrGdGa_3O_7$, $SrLaGa_3O_7$ and $BaLaGa_3O_7$ possess high piezoelectric coefficients (d_{14} = 14.5, 13.7, 12.3 pC/N, respectively), [9,13], which are much larger than those of quartz (d_{11} = 2.3 pC/N), $GaPO_4$ (d_{11} = 4.5 pC/N) and $La_3Ga_5SiO_{14}$ (LGS) (d_{11} = 6.3 pC/N) [14–16]. $Ca_2Al_2SiO_7$, likewise, as a member of the melilite family, exhibits a high resistivity on the order of 10^7 Ω·cm at 600 °C, which is two orders of magnitude higher than that of LGS crystals, indicating its advantages for high temperature sensors [14,17]. However, up to now, there have been no piezoelectric reports on their homogenous compound $CaYAl_3O_7$ crystal, which is therefore the research target of this work.

$CaYAl_3O_7$ (abbreviated as CYAM) single crystal, a member of the melilite family, possesses a high melting point of around 1630 °C with no phase transitions below the melting point [18]. In general, in view of the common physical properties, aluminate always possesses higher melting point and larger electrical resistivity than gallium oxide of the same type, which means that CYAM crystal may exhibit better piezoelectric performance and be more competitive for high temperature piezoelectric applications. In recent years, this compound has been studied for long lasting phosphorescence by doping Ce and Eu [19,20]. However, to date, limited investigations have been carried out on the temperature dependence of thermal, piezoelectric and related properties of this crystal. Therefore, it is high time to investigate the potential of CYAM single crystal as a new candidate for high temperature piezoelectric applications.

In this work, the thermal expansion and thermal conductivity were systematically investigated at elevated temperatures for piezoelectric sensing applications. Furthermore, the temperature dependence of the electrical resistivity, dielectric, piezoelectric, elastic constants and electromechanical coupling coefficient were investigated in the range of 25–500 °C.

2. Experimental

The crystals were grown by the Czochralski (Cz) technique using an automatic diameter control system with an RF induction heater. The synthesized polycrystalline materials were melted in an iridium crucible of $\Phi 60 \times 50$ mm^3 dimensions. Single crystals were grown with the <001> oriented seed crystals under Ar atmosphere. The pulling speed and rotation rate were set to be 0.6–1 mm/h and 15–25 rpm, respectively. After the growth process, the as grown crystals were cooled down to room temperature at a rate of 40~50 °C h^{-1}.

For micro-hardness measurement, a DHV-1000 digital micro tester (Shanghai Precision Instruments Co., Ltd., Shanghai, China) equipped with a diamond pyramidal indentor was employed. Polished wafers with dimensions of $4 \times 4 \times 1$ mm^3 were used for the measurements. The indentation load was stressed at a value of 50 g and the selected time was 10 s. Three test points were performed per sample to obtain the average value. The microhardness (Hv) and Mohs hardness (HM) values were calculated using the following equations [21]:

$$\mathrm{Hv} = 1.8544(\frac{P}{d^2})(\mathrm{kg\ mm^{-2}}) \tag{1}$$

$$\mathrm{HM} = 0.675(\mathrm{Hv})^{\frac{1}{3}} \tag{2}$$

where P is the applied load pressure and d is the diagonal length of the indentations.

The density of the CYAM crystal was measured by the Archimedes method and calculated according to the following equation:

$$\rho_0 = \frac{m_o \rho_{water}}{m_o - m_1} \tag{3}$$

where m_0 is the sample weight in air, m_1 is the sample weight immersed completely in distilled water, and ρ_{water} is the density of the distilled water at the measurement temperature (25 °C). Each density was determined by averaging the values of three samples in this experiment.

The linear thermal expansion coefficients of CYAM crystal were measured by a thermal mechanical analyzer (Mettler-Toledo Company, Zurich, Switzerland) in the temperature range of 25–500 °C. A cube crystal sample of $4 \times 4 \times 4$ mm^3 (a × a × c) was prepared from the as-grown crystals for the thermal expansion measurements.

The Perkin Elmer Diamond differential scanning calorimetry (Diamond DSC-ZC, Waltham, MA, USA) method was employed to determine the specific heat using a simultaneou thermal analyzer. The measurement temperature and heating rate were from 25 to 500 °C and 5 °C min^{-1} respectively. The thermal diffusivity was performed by a Netzsch Nanoflash model LFA 457 apparatus (Netzsch, Selb, Germany). Sample plates of (001) and (100) plates with the dimensions of $4 \times 4 \times 1$ mm^3 were cut from the as-grown crystal. The samples were coated with graphite on both the 4 × 4 mm^2 faces for even heating. When a short pulse heats one side of the sample, the temperature on the opposite surface is measured with an IR detector, from which the diffusivity coefficient is calculated. The temperature range is from 25 to 500 °C.

The electrical resistivity of X- and Z-direction was determined from the resistance, which was measured using a 2410 High-Voltage SourceMeter (Keithley, Cleveland, OH, USA) by applying 100 V on the two samples.

Belonging to the tetragonal space group $P\bar{4}2_1m$, CYAM crystal possesses 10 independent electro-elastic constants: two dielectric constants (ε_{11} and ε_{33}), six elastic constants (s_{11}, s_{12}, s_{13}, s_{33}, s_{55}, and s_{66}), and two piezoelectric constants (d_{14} and d_{36}).

Six CYAM crystal samples were prepared according to the Institute of Electrical and Electronics Engineers (IEEE) standard on piezoelectricity [22]. Table 1 lists the specimen orientations and shapes for the corresponding elastic and piezoelectric coefficients and the effective electromechanical coupling factors.

The capacitance of *X*- and *Z*-cut square plates at 1 kHz, as well as the resonance (f_r) and antiresonance (f_a) frequencies were measured using an Agilent 4294A type LCR (Agilent, CA, USA). Based on the measured capacitance, f_a and f_r values, the complete sets of dielectric, elastic and piezoelectric coefficients for the CYAM crystal were calculated. Additionally, the first, second, and third order temperature coefficients of the elastic compliance constants were calculated according to the following equations [22,23]:

$$T_{s_{ij}}^{(1)} = \frac{1}{s_{ij0}} \frac{\partial s_{ij}}{\partial T}\bigg|_{T=T_0} \tag{4}$$

$$T_{s_{ij}}^{(2)} = \frac{1}{2s_{ij0}} \frac{\partial s_{ij}}{\partial T}\bigg|_{T=T_0} \tag{5}$$

$$T_{s_{ij}}^{(3)} = \frac{1}{6s_{ij0}} \frac{\partial s_{ij}}{\partial T}\bigg|_{T=T_0} \tag{6}$$

where s_{ij0} is the elastic coefficient at the temperature $T = T_0$.

Table 1. Effective elastic and piezoelectric constants for different specimens.

Specimen	Electric Field Direction	Coefficients
X-cut square plate	*X*	ε_{11}, $s_{44} = s_{55}$
Z-cut square plate	*Z*	ε_{33}, s_{66}
(*XY*t)5° (*XY*t)45° and (*XY*t)85° bars	*X*	s_{11}, s_{33}, $2s_{13} + s_{55}$, d_{14}, k_{36}
(*ZX*t)45° bar	*Z*	$2s_{12} + s_{66}$, d_{36}, k_{14}

3. Results and Discussion

As is shown in Table 2, the H*v* hardness values of the <100> and <001> oriented samples for the $CaYAl_3O_7$ crystal were found to be 1188 and 833 kg mm^{-2}, respectively, with the Mohs hardness values being on the order of 7.14 and 6.35, respectively. By comparison, the <100> oriented hardness values are larger than the <001> oriented one. This phenomenon is contributed to the anisotropic effects of crystal. The atomic arrangement inside the sheet layer (<100> direction) is much closer than that along the <001>-direction, therefore, stronger interatomic forces are associated with a larger hardness.

The density of $CaYAl_3O_7$ at room temperature measured by the Archimedes method was found to be 3.61 ± 0.01 g/cm^3, which is consistent with the calculated value based on XRD results, namely, 3.60 g/cm^3.The density values at different temperatures were calculated based on the thermal expansion coefficients according to the following formula:

$$\rho = \frac{m}{abc} = \frac{m}{a_0 b_0 c_0 \left(1+\frac{\Delta a}{a_0}\right)\left(1+\frac{\Delta b}{b_0}\right)\left(1+\frac{\Delta c}{c_0}\right)} = \frac{\rho_0}{\left(1+\frac{\Delta a}{a_0}\right)\left(1+\frac{\Delta b}{b_0}\right)\left(1+\frac{\Delta c}{c_0}\right)} \tag{7}$$

where ρ_0 is the density at room temperature, the value of $\Delta a/a = \Delta b/b$ and $\Delta c/c$ can be obtained from the corresponding thermal expansion curves, as illustrated in Figure 1, the density of crystal decreases linearly from 3.61 to 3.54 g/cm^3 over the range of 25–500 °C.

Table 2. Microhardness (Hv) hardness and Mohs hardness.

	$CaYAl_3O_7$	
	<100>	<001>
Hv (kg/mm^2)	1188	833
HM	7.14	6.35

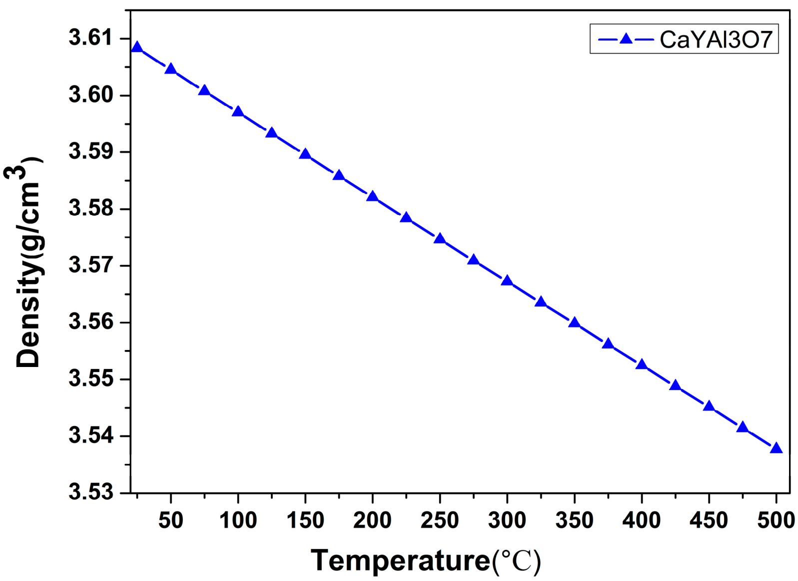

Figure 1. Density as a function of temperature for $CaYAl_3O_7$ (CYAM) crystal.

The thermal expansion coefficient α_{ij} of a crystal is a symmetric second-rank tensor. As the $CaYAl_3O_7$ crystal has a tetragonal system, there are two independent thermal expansion coefficients, α_{11} and α_{33} ($\alpha_{11} = \alpha_a$, $\alpha_{33} = \alpha_c$). The average thermal expansion coefficient can be calculated according to the following equation [24]:

$$\overline{\alpha}(T_0 \to T) = \frac{\Delta L}{L_0}\frac{1}{\Delta T} \tag{8}$$

where $\overline{\alpha}(T_0 \to T)$ is the average thermal expansion coefficient over the temperature range from T_0 to T, L_0 is the sample length at T_0, ΔL is the length exchange when the temperature changes from T_0 to T, and $\Delta T = (T - T_0)$ is the temperature exchange value. As can be seen from Figure 2, these two thermal expansion curves are increased linearly without any significant deviation within the measuring temperature range from 25 °C to 500 °C. The linear thermal expansion coefficients were calculated to be: $\alpha_a = 6.63 \times 10^{-6}$ K^{-1} and $\alpha_c = 28.52 \times 10^{-6}$ K^{-1}, where the α_c is much higher than that of α_a, due to the fact that the weak Ca-O and Y-O bonds along the Z direction contribute greatly to the thermal expansion, while inside the XY-plane, strong interatomic forces result in a lower thermal expansion [19].

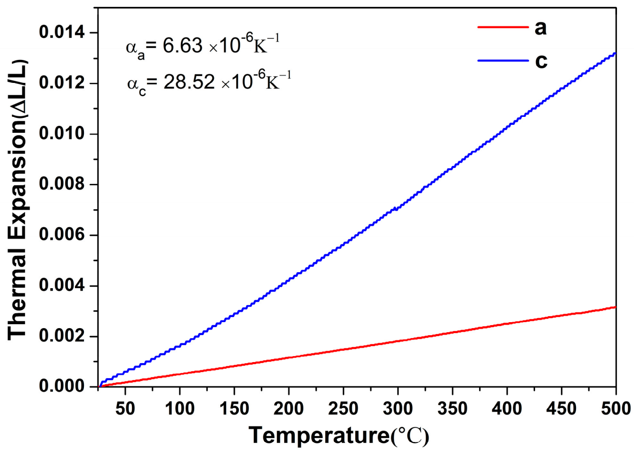

Figure 2. The thermal expansion of CYAM crystal along a and c axes.

Based on the thermal diffusivity and specific heat, the thermal conductivity can be calculated by using the equation $k = \lambda \cdot \rho \cdot C_p$, where λ, ρ, C_p denote the thermal diffusion coefficient, density and specific heat, respectively. The thermal conductivity of CYAM crystal was calculated as a function of temperature and depicted in Figure 3. The thermal conductivities of $CaYAl_3O_7$ along the a and c direction at room temperature were 1.82 and 1.37 $W \cdot m^{-1} \cdot K^{-1}$ respectively. As can be seen, the thermal conductivity increases with increasing temperature. This phenomenon indicates that the CYAM crystal can tolerate more thermal load at high temperature.

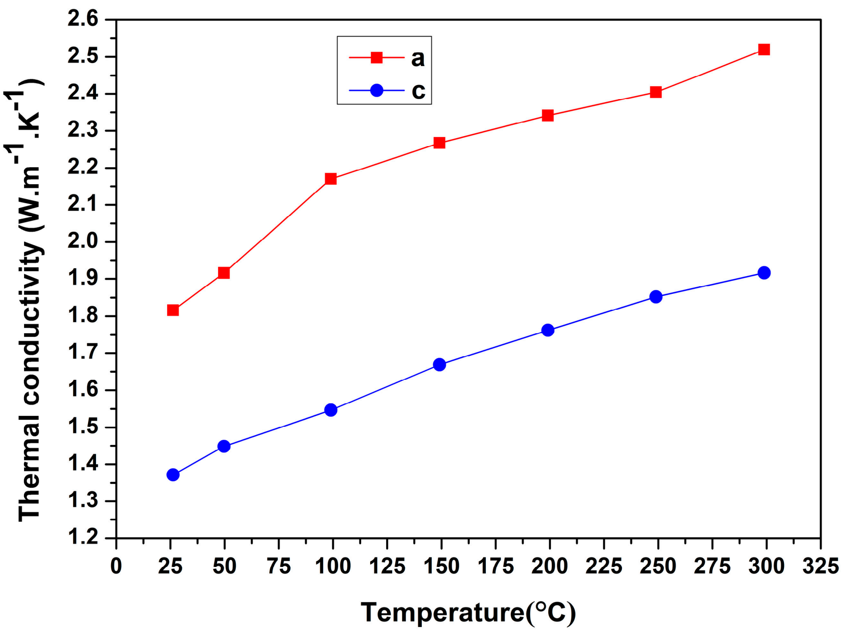

Figure 3. The thermal conductivity of CYAM crystal along a and c axes.

High resistivity at high temperature is beneficial to reduce the electrical losses and to improve the signal/noise ratio of sensors. Figure 4 gives the anisotropy of electrical resistivity and the temperature-dependent behaviors of electrical resistivity for CYAM crystal. In general, the resistivity decreases exponentially with the increase of temperature, as seen in the linear character of the curves in the Arrhenius plot, which is expressed by the Arrhenius law as follows:

$$\rho = \rho_0 \exp\left(\frac{E_a}{k_B T}\right) \tag{9}$$

where ρ_0 is the ultimate resistivity at an infinite temperature, k_B is the Boltzmann constant, T is the absolute temperature, and E_a is the activation energy, which can be determined from the logarithm plot of ρ vs. reciprocal temperature 1000/T, reflects the slope of the curves. The calculated E_a values of the CYAM crystal along X- and Z- direction are 1.11 and 1.10 eV, respectively. As can be seen, the resistivity along Z-direction is an order of magnitude larger than the value along X-direction, due to the AlO_4 layered crystal structure, where the layers are linked by high density interconnected antiprisms vertical to the Z-direction, giving rise to higher conductivity along the X-direction than that along the Z-direction [19]. In particular, the electrical resistivity along the X-axis and Z-axis were found to be 6.96×10^7 Ω·cm and 2.86×10^8 Ω·cm at 600 °C, respectively, which are comparable to $Ca_2Al_2SiO_7$ (10^8 Ω·cm at 600), and which are much larger than those of $LiNO_3$ crystals (1.2×10^5 Ω·cm) and LGS (2.5×10^5 Ω·cm) at the same temperature. This demonstrates the advantages of CYAM crystal for high temperature piezoelectric applications.

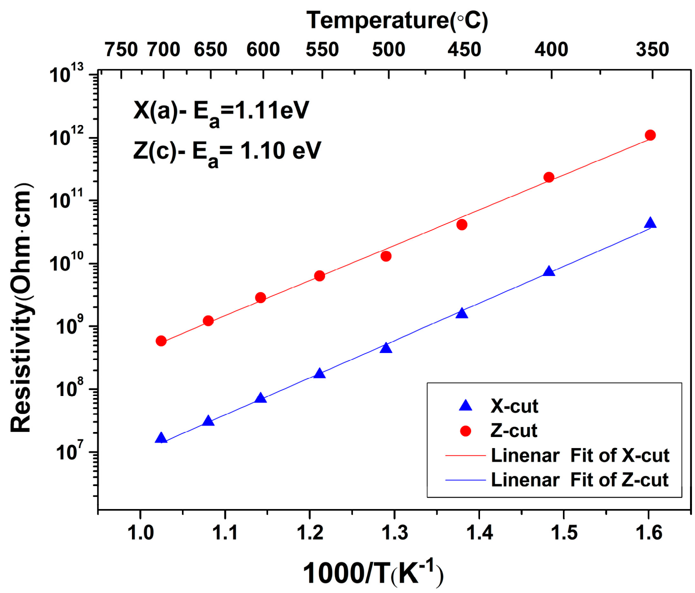

Figure 4. Temperature dependence of the resistivity of grown CYAM crystal.

In order to characterize the temperature stability of CYAM piezoelectric crystal, temperature dependence of the dielectric and electro-elastic constants was investigated systematically.

The temperature dependence of the dielectric constant ($\varepsilon_{ij}/\varepsilon_0$) and dielectric loss (tan δ) at 1 kHz as a function of temperature for CYAM crystal along the X- and Z- axes is depicted in Figure 5. As can be seen, the dielectric permittivity values $\varepsilon_{11}/\varepsilon_0$ and $\varepsilon_{33}/\varepsilon_0$ were found to increase slightly with increasing temperature, and the corresponding dielectric loss (shown in the Figure 5) is steady around 1% from room temperature to 450 °C, and then it increases rapidly to ~2.5% at 500 °C.

Understanding of the temperature dependence of the elastic constants is also quite important for the application of crystals. The temperature dependent elastic compliance s_{ij} of CYAM crystals is shown in Figure 6. With an increase in temperature, the values of s_{ij} exhibit a very stable state in the temperature range of 25~500 °C. It is concluded that the crystal exhibits high thermal stability of elastic constant with variation less than 4%. As can be seen from Table 3, the first-, second-, and third-order temperature coefficients of the elastic coefficients have been shown by using equations below, indicating that CYAM has superior temperature stability.

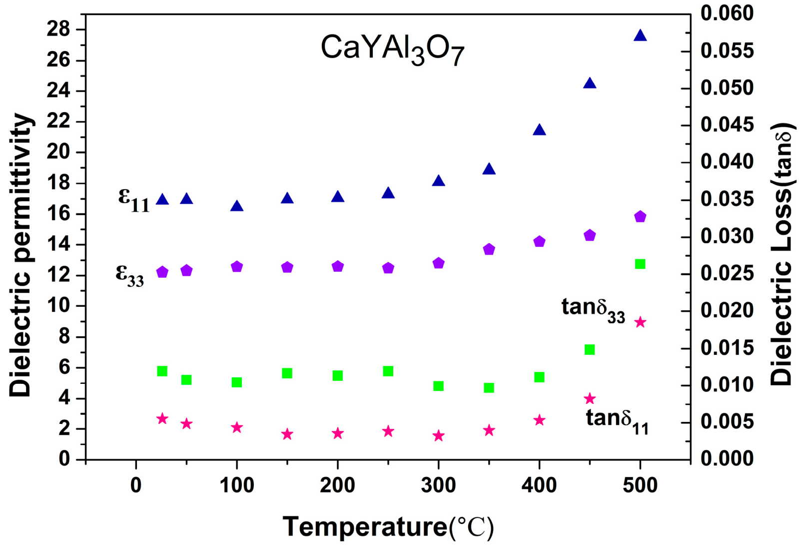

Figure 5. Dielectric permittivity and dielectric loss (tan δ) of CYAM crystal as a function of temperature.

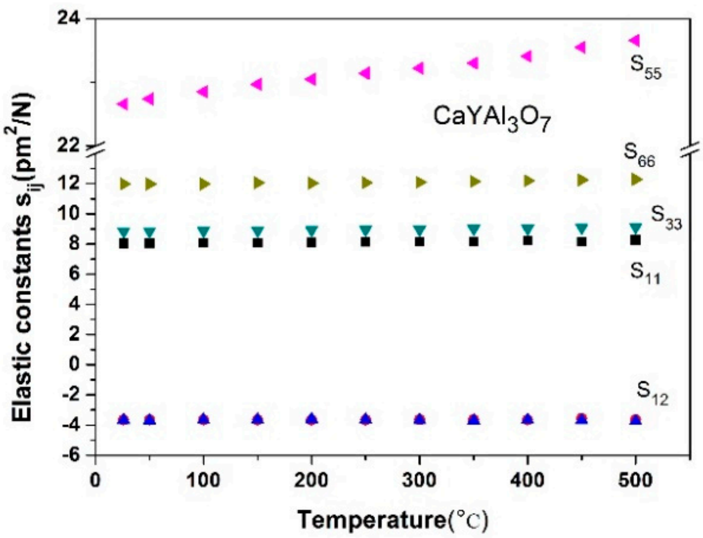

Figure 6. Temperature dependence of the elastic compliance of CYAM crystal.

Table 3. First-, Second-, and Third-Order Temperature Coefficients of the Elastic Constants.

	Ts_{11}	Ts_{12}	Ts_{13}	Ts_{33}	Ts_{55}	Ts_{66}
first order $10^{-6}/°C$	442	144	164	670	2820	−53
second order $10^{-9}/°C^2$	−255	−29	136	−1110	−4285	1846
third order $10^{-12}/°C^3$	751	−43	228	1992	5718	−962

Figure 7 shows the piezoelectric coefficient variation as a function of temperature. The piezoelectric coefficients of d_{36} maintained similar values in the range of 25~500 °C, while d_{14} increased slightly from 12.56 to 14.94 pC/N over the temperature range of 25~500 °C, with the variations being less than 19%.

The temperature dependence of the electromechanical coupling factors k_{14} and k_{36} was also measured, as shown in Figure 8. The electromechanical coupling k_{14} and k_{36} were found to be 18.28% and 5.36% at 500 °C, respectively. As expected, the variation tendency of the coupling factors is similar to that of the piezoelectric coefficients, increasing slightly with increasing temperature with total variation of less than 4%.

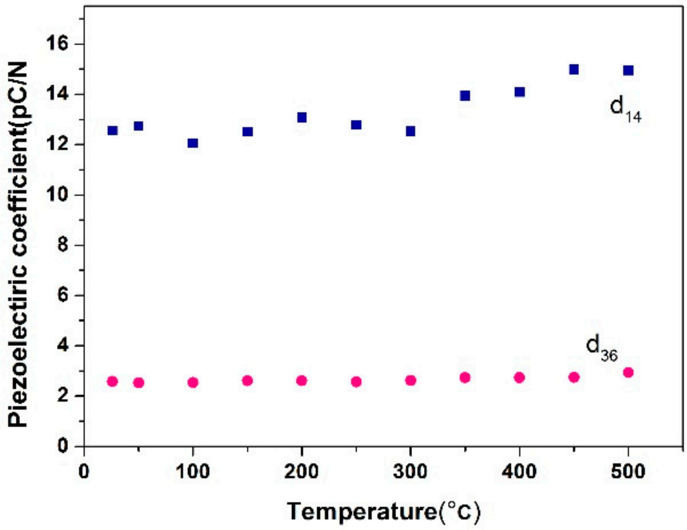

Figure 7. Temperature dependent piezoelectric coefficient of CYAM crystal.

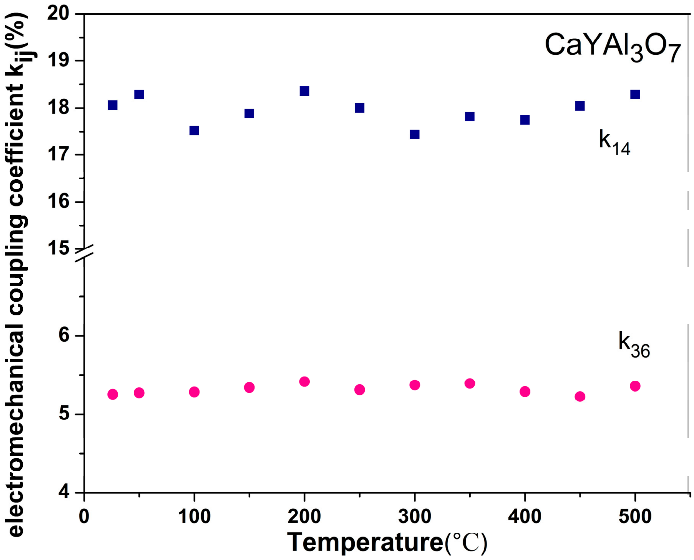

Figure 8. Electromechanical coupling factor of CYAM crystal as a function of temperature.

4. Conclusions

In summary, the temperature dependence of electrical resistivity, dielectric and piezoelectric, elastic properties of $CaYAl_3O_7$ crystal are reported. The fundamental properties, including hardness, density and thermal properties have also been systematically measured. The density was measured to be 3.61 g/cm^3, which was in good agreement with the theoretical value. The thermal expansion coefficients were calculated to be $\alpha_a = 6.63 \times 10^{-6}$ K^{-1} and $\alpha_c = 28.52 \times 10^{-6}$ K^{-1}. It is notable that the electrical resistivity for CYAM crystal was over 10^7 Ω·cm along both the *X*- and *Z* directions at 600 °C, which are much larger than those of $LiNO_3$ crystals (1.2×10^5 Ω·cm) and LGS (2.5×10^5 Ω·cm).

This investigation concerning the temperature dependence in respects of the dielectric, elastic and piezoelectric properties of CYAM crystal shows an excellent thermal stability. Based on the high temperature stability of its resistivity and piezoelectric properties, together with the high melting point (~1630 °C), $CaYAl_3O_7$ single crystal is an excellent candidate for piezoelectric sensors.

Acknowledgments: We gratefully acknowledge the financial support from the National Natural Science Foundation of China (Grant No. 51321091, 51772170 and 51323002) and the Young Scholars Program of Shandong University (Grant No. 2015WLJH36).

Author Contributions: Xiaoqiang Yu and Xutang Tao conceived and designed the experiments. Qiangqiang Hu and Yang Li performed the growth of the single crystal; Wenxiang Mu performed the thermal experiments and analyzed the data. Yang Li and Yanru Yin accomplished the electrical resistivity and high temperature piezoelectric measurements; Jian Zhang collected the single-crystal X-ray diffraction data and solved the structures; Zhitai Jia and Yang Li wrote the paper.

Conflicts of Interest: The authors declare no conflict of interest.

References

1. Zhang, S.; Yu, F.; Green, D.J. Piezoelectric materials for high temperature sensors. *J. Am. Ceram. Soc.* **2011**, *94*, 3153–3170. [CrossRef]
2. Zhang, S.; Zheng, Y.; Kong, H.; Xin, J.; Frantz, E.; Shrout, T.R. Characterization of high temperature piezoelectric crystals with an ordered langasite structure. *J. Appl. Phys.* **2009**, *105*, 114107. [CrossRef]
3. Shrout, T.R.; Zhang, S.J. Lead-free piezoelectric ceramics: Alternatives for PZT? *J. Electroceram.* **2007**, *19*, 113–126. [CrossRef]
4. Fu, H.; Cohen, R.E. Polarization rotation mechanism for ultrahigh electromechanical response in single-crystal piezoelectrics. *Nature* **2000**, *403*, 281. [CrossRef] [PubMed]
5. Zhang, S.-T.; Kounga, A.B.; Aulbach, E.; Deng, Y. Temperature-dependent electrical properties of $0.94Bi_{0.5}Na_{0.5}TiO_3$–$0.06BaTiO_3$ ceramics. *J. Am. Ceram. Soc.* **2008**, *91*, 3950–3954. [CrossRef]
6. Baba, A.; Searfass, C.T.; Tittmann, B.R. High temperature ultrasonic transducer up to 1000 °C using lithium niobate single crystal. *Appl. Phys. Lett.* **2010**, *97*, 232901. [CrossRef]
7. Turner, R.C.; Fuierer, P.A.; Newnham, R.E.; Shrout, T.R. Materials for high temperature acoustic and vibration sensors: A review. *Appl. Acoust.* **1994**, *41*, 299–324. [CrossRef]
8. Fritze, H.; Tuller, H.L. Langasite for high-temperature bulk acoustic wave applications. *Appl. Phys. Lett.* **2001**, *78*, 976–977. [CrossRef]
9. Shen, C.; Zhang, Y.; Yu, H.; Zhang, S.; Cao, W.; Wang, J.; Zhang, H. Dielectric, elastic and piezoelectric properties of $SrLaGa_3O_7$ and $BaLaGa_3O_7$ crystals with melilite structure. *J. Alloys Compd.* **2015**, *647*, 1069–1074. [CrossRef]
10. Smith, R.T.; Welsh, F.S. Temperature dependence of the elastic, piezoelectric, and dielectric constants of lithium tantalate and lithium niobate. *J. Appl. Phys.* **1971**, *42*, 2219–2230. [CrossRef]
11. Xia, H.; Feng, J.; Wang, Y.; Li, J.; Ji, Y.; Jia, Z.; Tu, C. The effects of Ho^{3+} and Pr^{3+} ions on the spectroscopic properties of Er^{3+} doped $SrGdGa_3O_7$ crystals used in mid-infrared lasers. *J. Phys. D Appl. Phys.* **2015**, *48*, 435106. [CrossRef]
12. Shen, C.; Zhang, S.; Wang, D.; Xu, T.; Yu, H.; Cao, W.; Wang, J.; Zhang, H. Growth and property characterization of $CaNdGa_3O_7$ and $SrNdGa_3O_7$ melilite single crystals. *CrystEngComm* **2015**, *17*, 1791–1799. [CrossRef]
13. Zhang, Y.; Yin, X.; Yu, H.; Cong, H.; Zhang, H.; Wang, J.; Boughton, R.I. Growth and piezoelectric properties of melilite ABC_3O_7 crystals. *Cryst. Growth Des.* **2012**, *12*, 622–628. [CrossRef]
14. Shimamura, K.; Takeda, H.; Kohno, T.; Fukuda, T. Growth and characterization of lanthanum gallium silicate $La_3Ga_5SiO_{14}$ single crystals for piezoelectric applications. *J. Crys. Growth* **1996**, *163*, 388–392. [CrossRef]
15. Philippot, E.; Ibanez, A.; Goiffon, A.; Cochez, M.; Zarka, A.; Capelle, B.; Schwartzel, J.; Détaint, J. A quartz-like material: Gallium phosphate ($GaPo_4$); crystal growth and characterization. *J. Cryst. Growth* **1993**, *130*, 195–208. [CrossRef]
16. Tichý, J.; Privatska, J.; Prívratská, J.; Kittinger, E.; Erhart, J.; Janovec, V. Fundamentals of piezoelectric sensorics : Mechanical, dielectric, and thermodynamical properties of piezoelectric materials. *Cheminform* **2010**, *34*, 1423–1440.

17. Hagiwara, M.; Noguchi, H.; Hoshina, T.; Takeda, H.; Fujihara, S.; Kodama, N.; Tsurumi, T. Growth and characterization of $Ca_2Al_2SiO_7$ piezoelectric single crystals for high-temperature sensor applications. *Jpn. J. Appl. Phys.* **2013**, *52*, 09KD03. [CrossRef]
18. Philippen, J.; Guguschev, C.; Klimm, D. Single crystal fiber growth of cerium doped strontium yttrate, SrY_2O_4:Ce^{3+}. *J. Cryst. Growth* **2017**, *459*, 17–22. [CrossRef]
19. Park, S.H.; Lee, K.H.; Unithrattil, S.; Yoon, H.S.; Jang, H.G.; Im, W.B. Melilite-structure $CaYAl_3O_7$:Eu^{3+} phosphor: Structural and optical characteristics for near-UV led-based white light. *J. Phys. Chem. C Nanomater. Interfaces* **2012**, *116*, 26850–26856. [CrossRef]
20. Kodama, N.; Takahashi, T.; Yamaga, M.; Tanii, Y.; Qiu, J.; Hirao, K. Long-lasting phosphorescence in Ce^{3+}-doped $Ca_2Al_2SiO_7$ and $CaYAl_3O_7$ crystals. *Appl. Phys. Lett.* **1999**, *75*, 1715–1717. [CrossRef]
21. Yuan, D.; Jia, Z.; Wang, J.; Gao, Z.; Zhang, J.; Fu, X.; Shu, J.; Yin, Y.; Hu, Q.; Tao, X. Bulk growth, structure, and characterization of the new monoclinic $TbCa_4O(BO_3)_3$ crystal. *CrystEngComm* **2014**, *16*, 4008–4015. [CrossRef]
22. Meitzler, A.H.; Berlincourt, D.; Welsh, F.S.; Tiersten, H.F.; Coquin, G.A.; Warner, A.W. *176-1987 IEEE Standard on Piezoelectricity*; IEEE: Piscataway, NJ, USA, 1988.
23. Gao, Z.; Yin, X.; Zhang, W.; Wang, S.; Jiang, M.; Tao, X. Temperature dependence of elastic properties and piezoelectric applications of $BaTeMo_2O_9$ single crystal. *IEEE Trans. Ultrason. Ferroelectr. Freq. Control* **2011**, *58*, 2753. [CrossRef] [PubMed]
24. Hu, Q.; Jia, Z.; Tang, C.; Lin, N.; Zhang, J.; Jia, N.; Wang, S.; Zhao, X.; Tao, X. The origin of coloration of $CaGdAlO_4$ crystals and its effect on their physical properties. *CrystEngComm* **2017**, *19*, 537–545. [CrossRef]